



Fluidisable mesoporous silica composites for thermochemical energy storage

Haomin Wang, Xin Liu **, Xiao Liu, Chenggong Sun, Yupeng Wu *

Faculty of Engineering, University of Nottingham, Nottingham, NG7 2RD, United Kingdom

ARTICLE INFO

Keywords:

Thermochemical energy storage
Salt composites
Water adsorption
Salt hydrate
Mesoporous structure

ABSTRACT

Salt hydrate based thermochemical energy storage has been widely recognised as a promising long-duration storage technology to decarbonize heating/cooling in buildings. However, currently there are few salt hydrate-based energy storage materials capable to fulfil the requirements for energy density, efficiency, scalability and stability due to inappropriate particle size of the material. In this study, a commercially available mesoporous silica with large pore volume and good fluidisability was used as the porous matrix to prepare salt composites containing different salts (CaBr_2 , MgBr_2 , MgSO_4 , CaCl_2 , and $\text{Al}(\text{NH}_4)(\text{SO}_4)_2$) via a facile incipient wetness impregnation method. A variety of techniques including scanning electron microscopy (SEM), transmission electron microscopy (TEM), X-ray powder diffraction (XRD), nitrogen physisorption measurements and thermogravimetric analysis (TGA) were used to characterize the physicochemical properties and water hydration/dehydration performance of mesoporous silica-based salt composites. The results showed that both salt loading level and salt type play critical roles in determining the water adsorption performance of salt composites. Tested under hydration conditions of 30 °C and vapour pressure of 25 mbar, the CaCl_2 based salt composites exhibited the highest water adsorption capacity, which reached 109 wt% at the CaCl_2 loading level of 50 wt%, while the MgBr_2 based salt composites had faster water adsorption rates than other salt composites. Most of the salt composites were capable of desorbing 70–80% of the adsorbed water at temperatures below 90 °C, highlighting their great potential to store low-grade heat such as industrial waste heat or solar thermal energy. Advanced characterization demonstrated that the large pore volume and pore size improved the salt molecules' accessibility and water diffusivity inside the pores, leading to high water adsorption capacity and fast hydration/dehydration rate. In the aspects of particle size for future upscaling, this work presents an all new scalable and fluidisable salt composite material that opens up the potential to develop low-temperature fluidised bed based thermal energy storage systems for the first time.

1. Introduction

Currently, the building sector accounts for almost one-third of global final energy consumption, and space heating/cooling accounts for 60% of global carbon dioxide emissions in this sector [1]. Decarbonising heat in buildings has been identified as a key pillar of achieving 26th UN Climate Change Conference of the Parties (COP26) goals of securing global net-zero by mid-century. However, the building sector is challengeable to be decarbonised due to its diversity, complexity and extreme seasonality for heat requirements. Thermal energy storage (TES) has been considered as the most viable solution that can help to reduce the heating demand from immediate power, mitigate the

mismatch in heating demand and supply, and also support the shift to a predominantly renewable-based energy [2,3]. In short, TES has the potential to achieve a deep reduction in carbon emissions from heating in the short-to-medium term.

Among various thermal energy storage technologies developed, thermochemical energy storage (TCES), which uses reversible physical/chemical reactions to store large quantities of heat, offers enormous potential owing to its wide operating temperature range, high volumetric energy density and long term heat storage with negligible heat losses [4,5]. Salt hydrates based TCES that involve reversible endothermal and exothermal reactions between salt and water molecules at low temperatures, have been considered as a potential candidate for supplying heating in buildings. Various salts such as MgSO_4 [6,7], MgCl_2

* Corresponding author.

** Corresponding author.

E-mail addresses: Xin.Liu@nottingham.ac.uk (X. Liu), yupeng.wu@nottingham.ac.uk (Y. Wu).

<https://doi.org/10.1016/j.energy.2023.127255>

Received 21 November 2022; Received in revised form 2 March 2023; Accepted 17 March 2023

Available online 24 March 2023

0360-5442/© 2023 The Authors. Published by Elsevier Ltd. This is an open access article under the CC BY license (<http://creativecommons.org/licenses/by/4.0/>).

Nomenclature		K_1	Rate constant for first order equation
Abbreviations		K_2	Rate constant for second order equation
BET	Brunauer–Emmett–Teller	K_a	Rate constant for Avrami’s equation
BJH	Barrett–Joyner–Halenda	$m_{\text{anhydrous salt}}$	Mass of anhydrous salt (kg)
DFT	Density functional theory	$m_{\text{hydrated salt}}$	Mass of hydrated salt (kg)
DSC	Differential scanning calorimetry	$m_{\text{PQ silica}}$	Mass of PQ silica (kg)
PSD	Pore size distribution	$M_{\text{anhydrous salt}}$	Molar mass of anhydrous salt (g/mol)
SEM	Scanning electron microscopy	$M_{\text{hydrated salt}}$	Molar mass of hydrated salt (g/mol)
TCES	Thermochemical energy storage	n	Avrami’s exponent
TEM	Transmission electron microscopy	p	Purity of the purchased salt sample
TES	Thermal energy storage	q_e	Mass increase by moisture adsorption at equilibrium state (%)
TGA	Thermogravimetric analysis	q_t	Mass increase by moisture adsorption amount at time t (%)
XRD	X-ray diffraction	x	Time elapsed (s)
Symbols			
a	Salt loading amount for salt composite		

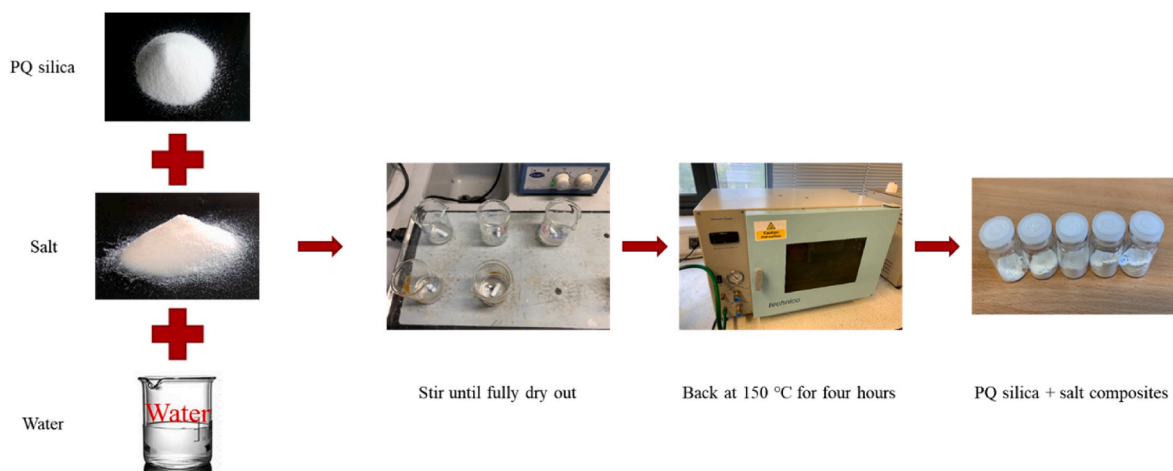


Fig. 1. Schematic diagram of the salt composites preparation process.

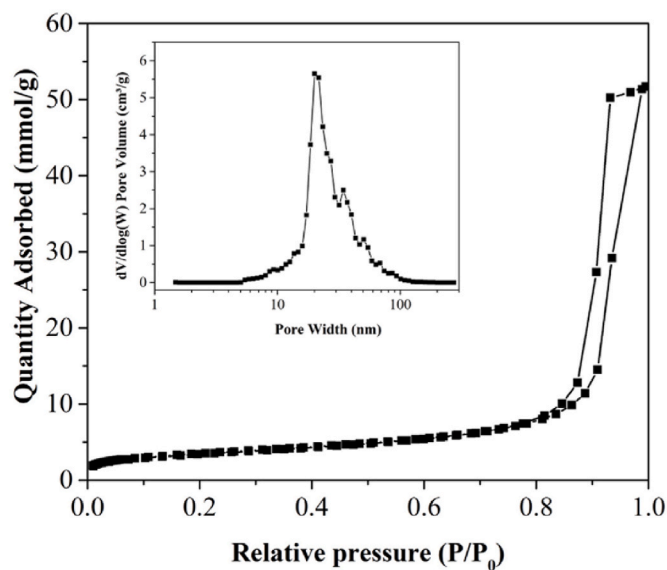


Fig. 2. Nitrogen adsorption isotherm at $-196\text{ }^{\circ}\text{C}$ and pore size distribution of PQ silica.

Table 1
Textural properties of PQ silica and its salt composites.

Salt	loading level (%)	Surface area (m ² /g)	Total pore volume (cm ³ /g)	Pore size (nm)
PQ silica	–	283	1.79	27.4
CaCl ₂	15	212	1.15	21.0
CaBr ₂		216	1.21	23.3
MgBr ₂		234	1.25	24.1
MgSO ₄		179	0.86	21.4
Al(NH ₄)(SO ₄) ₂		211	1.33	27.8
CaCl ₂	30	143	0.69	21.6
CaBr ₂		145	0.75	21.9
MgBr ₂		187	1.04	22.8
MgSO ₄		145	0.73	22.9
Al(NH ₄)(SO ₄) ₂		165	0.94	24.9
CaCl ₂	50	78	0.40	21.8
CaBr ₂		85	0.46	22.6
MgBr ₂		122	0.59	18.8
MgSO ₄		88	0.46	23.4
Al(NH ₄)(SO ₄) ₂		102	0.63	26.7

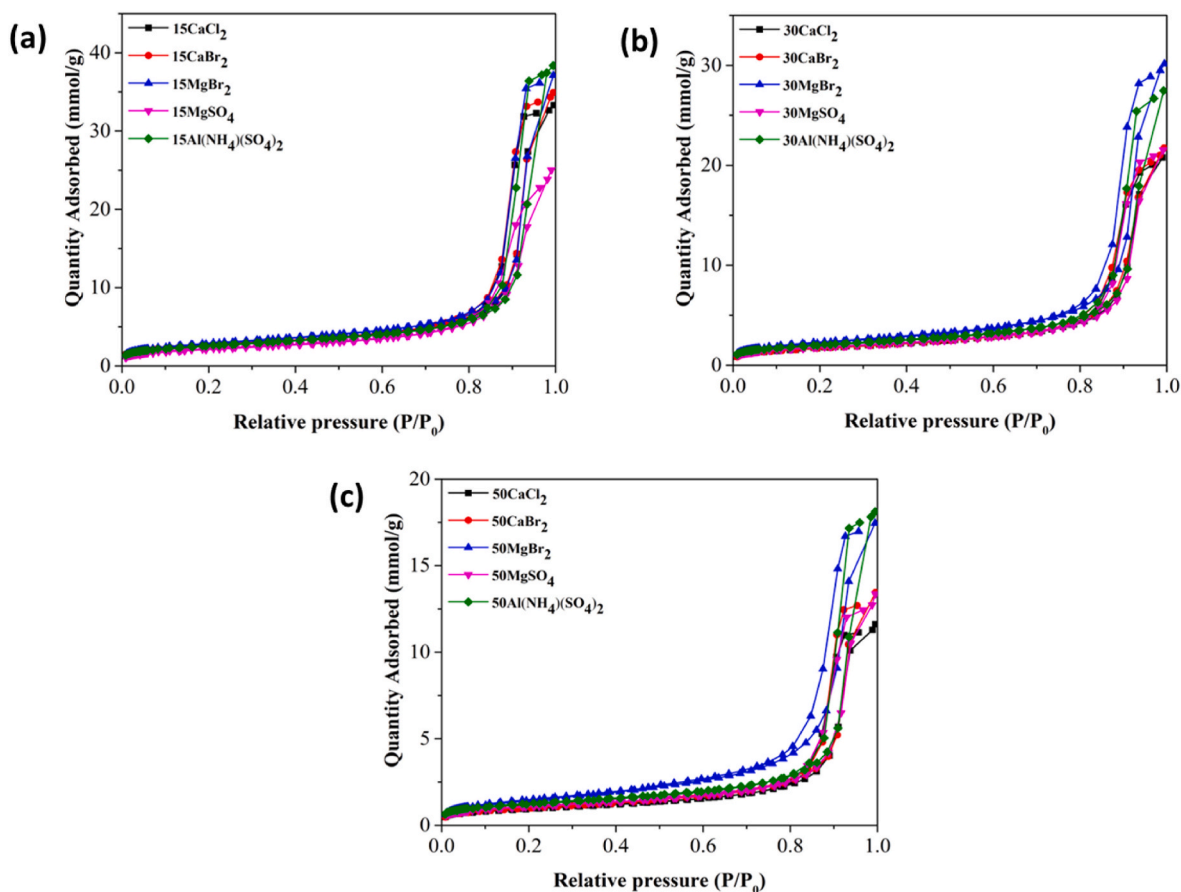


Fig. 3. Nitrogen adsorption isotherms at $-196\text{ }^{\circ}\text{C}$ of salt composites: (a) 15 wt% salt loading; (b) 30 wt% salt loading; (c) 50 wt% salt loading.

[8], and SrBr₂ [9] with high energy density in the range of 300–780 kWh/m³ [10–12] have been widely studied. In spite of large energy storage capacity, pure salt hydrates are subject to several restrictions for practical applications, such as easy deliquescence/agglomeration, and low thermal conductivity [13,14]. To circumvent these problems, one of the most important strategies is to impregnate salt in a porous matrix to prepare a new family of composites named ‘salt in porous matrix’ (CSPMs) [15,16]. Previous studies have demonstrated that the open channels inside the porous matrix benefit the dispersion and accessibility of salt molecules compared to bulk salt, leading to reduced moisture diffusion resistance and faster adsorption/desorption rate. Moreover, porous matrices can improve the cyclic stability of salt and prevent corrosion issues caused by salt. Numerous porous matrices including microporous materials (e.g. zeolite [17,18], activated carbon [19,20] and metal organic frameworks (MOFs) [21]), mesoporous materials (e.g. silica gel [22–25], Santa Barbara Amorphous-15 (SBA-15) [26], mesostructured cellular foam (MCF) [27]) and macroporous materials (e.g. glass bead [28]) have been investigated. Amongst different porous matrices, mesoporous materials have received increasing attention as their large pore sizes and pore volume can significantly improve the salt loading level and water diffusivity in pores, leading to both higher water adsorption capacity and faster adsorption kinetics, and therefore higher energy density. Previous studies have demonstrated that pore size and pore volume are critical to prepare salt composites. Liu et al. [27] reported the development of MgSO₄ based salt composite materials containing a large amount of MgSO₄ (up to 50 wt%) by using mesoporous silicas with different porous structure. Both water adsorption capacity and hydration/dehydration rate increased with increasing pore size and pore volume. Similarly, in Dawoud’s work [29], the composites prepared by using mesoporous silica with an average pore size of 15 nm achieved 22.8% faster in sorption rate and 19.2% higher in

moisture adsorption capacity than alumina based composites. Zheng et al. [30] reported that both water adsorption capacity and adsorption rate increased with increasing pore size of porous matrices from 2 to 10 nm. The salt molecules could lead to the blockage of small pores, reducing the accessibility of salt in pores and therefore the adsorption capacity and rate [31]. The above literature suggests that porous matrix with larger pore size and pore volume is preferable to prepare salt composites. Many investigations have been performed over recent years, but the pore size and pore volume of porous matrices tested in previous studies such as SBA-15 and silica gel have rarely exceeded 15 nm and 1 cm³/g, respectively, which capped the maximum salt loading level and the energy density of salt composites. Therefore, there is an urgent need to develop commercially available porous matrices with larger pore size and pore volume to prepare salt composites for thermochemical energy storage. In addition to the development of salt composites at the material level, the configuration of salt composite based TCES systems, especially the design of hydration/dehydration reactors, is also crucial. In general, there are four types of reactors available for salt composites including packed bed, moving bed, fluidised bed and entrained flow reactors. Amongst various reactors, fluidised bed reactors have received increasing attention owing to their better heat and mass transfer, uniform particle mixing, and lower gas velocities compared to other types of reactors [32,33]. To achieve successful fluidisation, the salt composite materials must meet the requirements of Geldart group A particles with particle sizes ranging from 30 to 125 μm and density on the order of 1500 kg/m³ or Geldart group B particles with particle sizes ranging from 150 to 1000 μm [34]. It has rarely been reported for low-temperature salt composites based TCES as most of the advanced porous matrices such as zeolite 13X [13,17,35] and silica gel [24,36,37] are either in the form of fine powder ($<1\text{ }\mu\text{m}$) or large beads ($>1000\text{ }\mu\text{m}$), making them difficult for fluidisation. Although those the hard-to-handle powder can

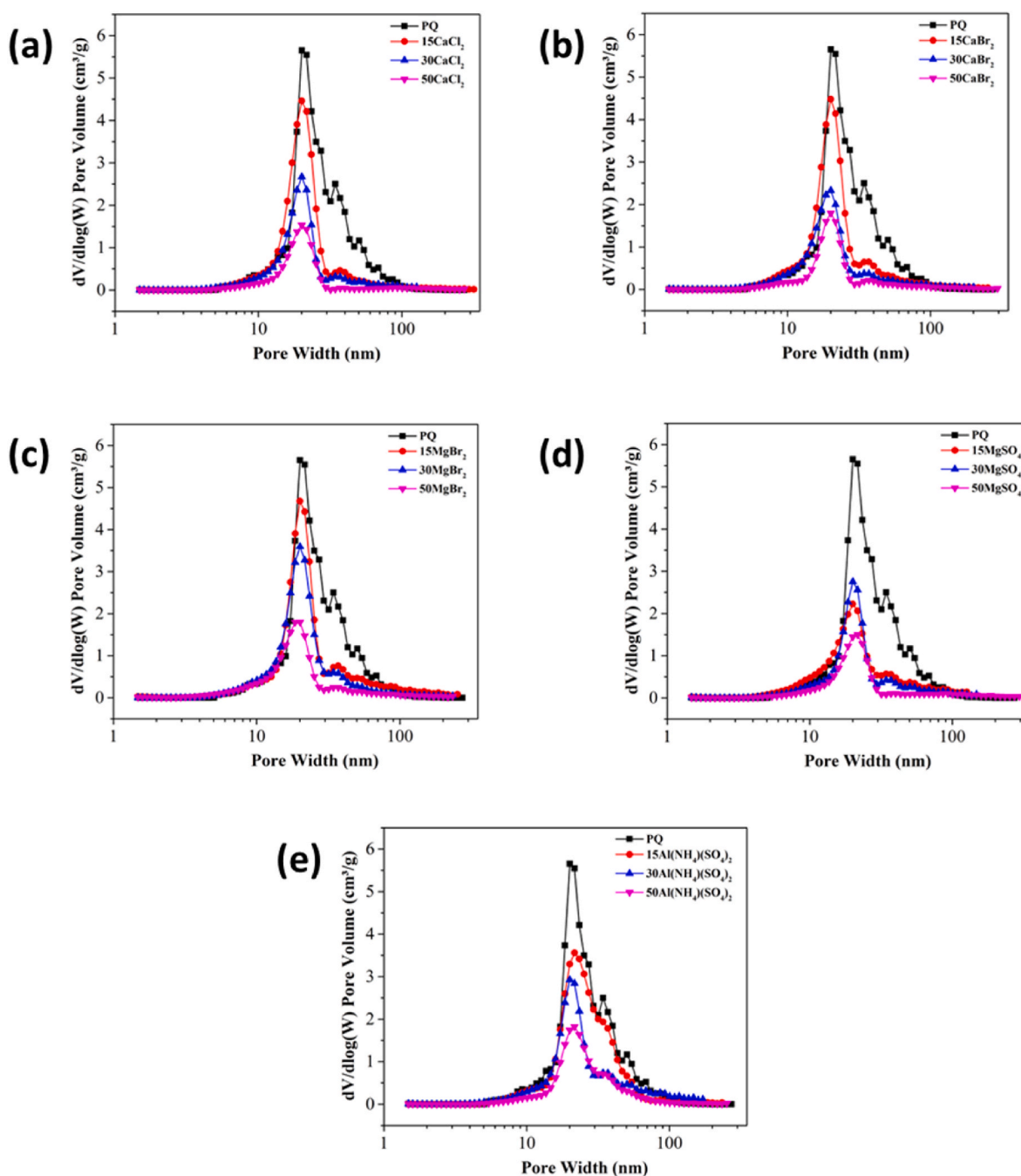


Fig. 4. Pore size distribution of salt composites: (a) CaCl_2 ; (b) CaBr_2 ; (c) MgBr_2 ; (d) MgSO_4 (e) $\text{Al}(\text{NH}_4)(\text{SO}_4)_2$.

be converted to pellets for packed bed reactors, the limited mass transfer within pellets can significantly reduce the water adsorption capacity and adsorption kinetics, and therefore dramatically decrease its energy efficiency [38]. Therefore, the development of fluidisable mesoporous matrices with large pore volume and pore size is of interest. In this study, a type of commercially available mesoporous silica with good fluidisability was selected as the porous matrix to prepare salt composites for thermochemical energy storage. By adopting this type of silica as the porous matrix, the composites can take the advantages from fluidised bed reactors for faster heat and mass transfer. In addition, previous studies were mainly focused on CaCl_2 and MgSO_4 , and there is limited research about other salts such as metal bromides and ammonium aluminium sulfate despite their large amount of crystal water. Five types of salts including CaBr_2 , MgBr_2 , MgSO_4 , CaCl_2 , and $\text{Al}(\text{NH}_4)(\text{SO}_4)_2$ were selected to prepare salt composites. The impact of salt types and

different salt loading levels on the water adsorption performance of the salt composites was studied.

2. Materials and methods

2.1. Preparation of salt composites

Commercial mesoporous silica was purchased from PQ SILICAS UK LIMITED. Calcium bromide hydrate, magnesium bromide hexahydrate, magnesium sulfate heptahydrate, calcium chloride anhydrous, and aluminium ammonium sulfate dodecahydrate were all purchased from Fisher Scientific. The salt composites were prepared via the incipient wet impregnation method [15,25]. In a typical procedure, the weighted PQ silica was added to 10 mL salt solution, and the mixture was magnetically stirred overnight. The white residual powder was dried in a

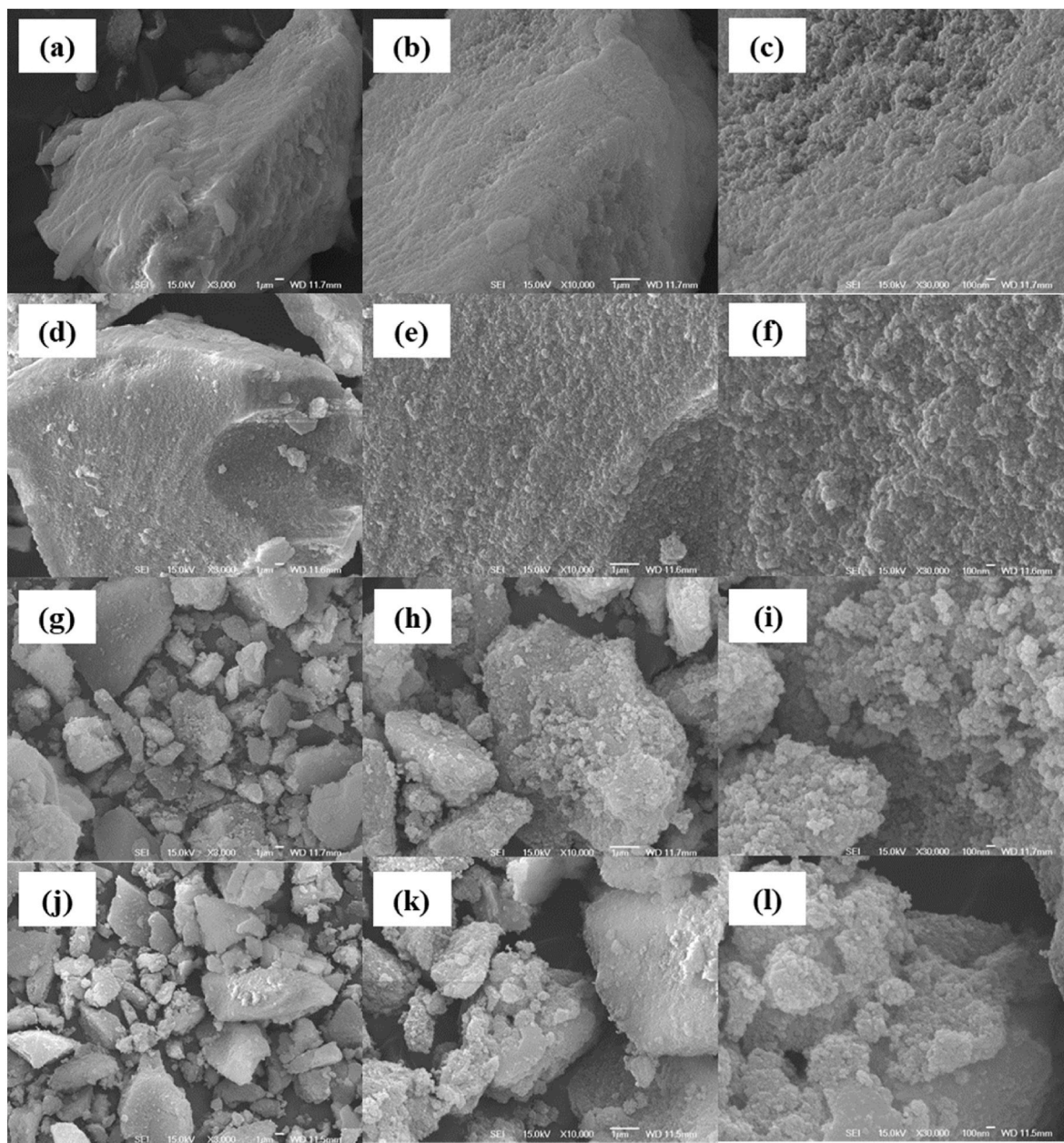


Fig. 5. SEM images of the selected salt composites at three different magnifications ($\times 3000$; $\times 10,000$ and $\times 30,000$): (a–c) 15 wt% CaCl_2 ; (d–f) 50 wt% CaCl_2 ; (g–i) 50 wt% MgBr_2 ; (j–l) 50 wt% MgSO_4 .

vacuum oven at 150°C for 4 hours. After drying, the white powder was collected and stored in a sealed bottle for the following experiments. The samples were labelled as ‘xSalt’, where ‘x’ represents the amount of salt impregnated into the PQ silica, and ‘Salt’ represents the type of salt impregnated. For the ease of comparison, the same salt impregnation amounts (15 wt%, 30 wt% and 50 wt%) were used for the preparation of the salt composites. Fig. 1 shows the composite preparation process via the incipient wet impregnation method.

2.2. Characterisation of porous matrix and salt composites

The morphological properties of PQ silica and its composites were imaged by JEOL 7000F Field Emission Gun Scanning Electron Microscopy (FEG-SEM) (JEOL Ltd, Japan). In order to further evaluate the CaCl_2 based composites, the transmission electron microscopy (TEM) was conducted with JEOL 2100 plus for PQ silica and selected salt composites. The instrument is operating at 200 kV, equipped with JEOL

STEM detectors and an Oxford Instruments XMax 100 TLE EDX detector. A Micrometrics ASAP 2420 was used to characterize the N_2 adsorption isotherm under the temperature of -196°C . Prior to the sorption tests, all samples were firstly degassed at 150°C for 16 hours. The specific area of the sample was tested by Brunauer, Emmett and Teller (BET) method. The pore size distribution was measured by Density functional theory (DFT). And the pore size was analysed by Barrett-Joyner-Halenda (BJH) method. The X-ray diffraction measurement (XRD) for 50 wt% salt composites was carried out on Bruker D8 Advance with DaVinci. Samples were scanned from 4 to 80° 2-theta, using a step size of 0.02° and a step time of 0.1 s, in Bragg-Brentano mode, using a 1D Lynxeye detector and a Cu X-ray tube.

2.3. Moisture adsorption/desorption measurements and analysis

The hydration and dehydration tests were carried out by thermal gravity analysis Q500 (TA instrument, USA) with the weighting accu-

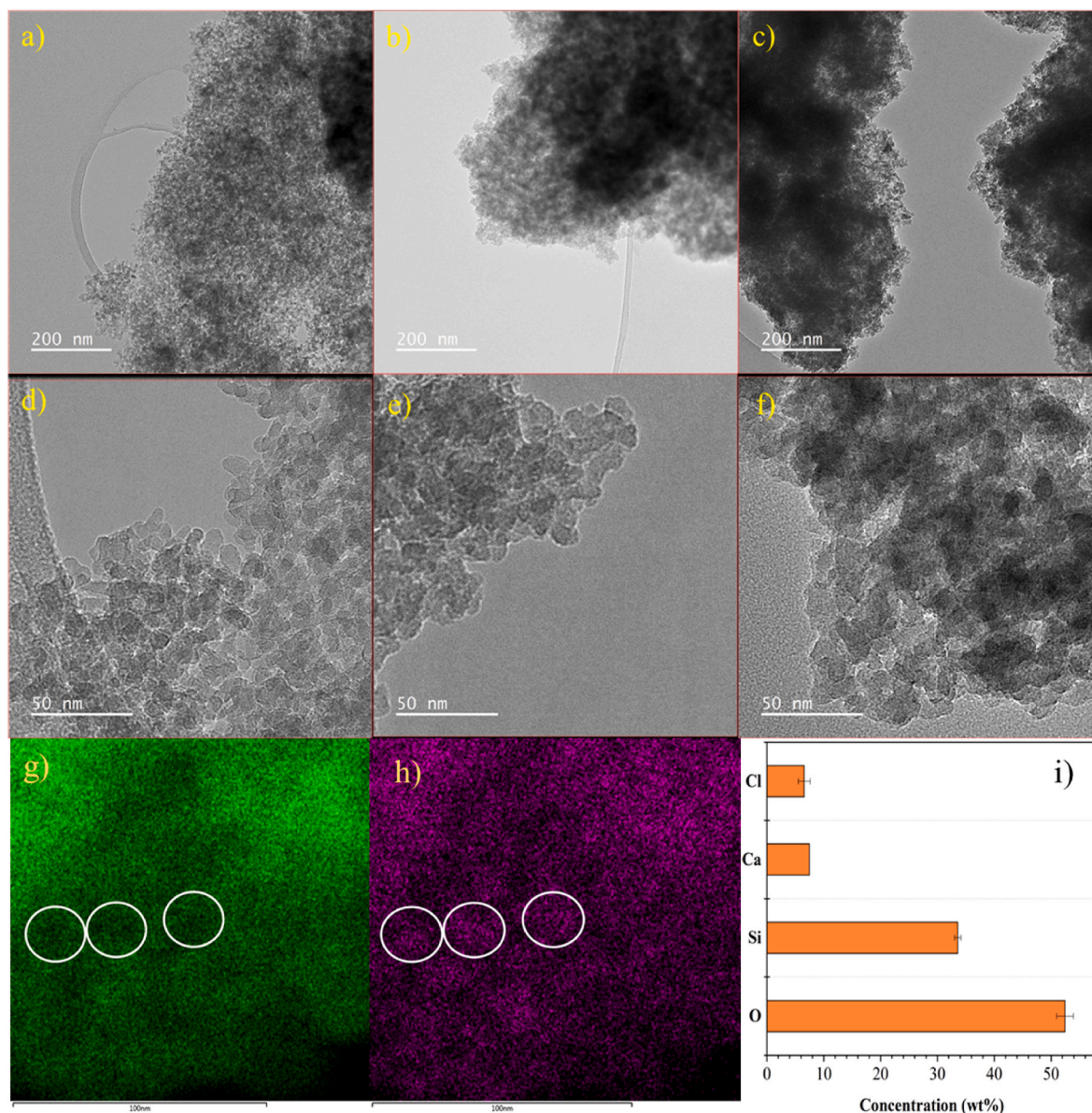


Fig. 6. TEM images of selected salt composites for: (a, d) PQ silica; (b, e) CaCl_2 composite with salt loading level of 30 wt%; (c, f) CaCl_2 composite with salt loading level of 50 wt%; (g) silicon mapping; (h) calcium mapping; (i) surface concentration of various elements. (For interpretation of the references to colour in this figure legend, the reader is referred to the Web version of this article.)

curacy of $\pm 0.1\%$, sensitivity of $0.1 \mu\text{g}$, and isothermal temperature accuracy of $\pm 1^\circ\text{C}$. Nitrogen was used as the purge gas with a flow rate of 100 mL/min . $20\text{--}40 \text{ mg}$ composite was used for each hydration/dehydration test. A typical cycle of hydration and dehydration includes pre-drying of the sample at 150°C for 45 min. Then the TGA sample chamber was cooled down to 30°C and supplied with moisture at 25 mbar water vapour pressure. Once the adsorption equilibrium was achieved, the sample was heated up again to 150°C with the heating rate of 1°C/min , and the moisture supply was stopped during the heating process. For the cycle stability test, these procedures are repeated for five times. In order to produce the salt composites with precise salt loading amount, the mass of salt sample should be calculated before mixing. The mass of anhydrous salt inside the composite can be calculated in Eq. (1).

$$m_{\text{anhydrous salt}} = (m_{\text{PQ silica}} \times a) / (1 - a) \quad (1)$$

where $m_{\text{PQ silica}}$ is the mass of PQ silica and a is the mass of anhydrous salt for salt composite. As some the purchased salts are in hydrated form,

it is necessary to convert the anhydrous salt to hydrated salt with Eq. (2).

$$m_{\text{hydrated salt}} = \frac{m_{\text{anhydrous salt}} \times M_{\text{hydrated salt}}}{M_{\text{anhydrous salt}} \times p} \quad (2)$$

where $M_{\text{hydrated salt}}$ is the molar mass of hydrated salt, $M_{\text{anhydrous salt}}$ is the molar mass of anhydrous salt and p is the purity of the purchased salt. The salt composite with precise salt loading amount can be produced by mixing the certain amount of hydrated salt sample and PQ silica calculated above.

2.4. Adsorption kinetic models

To better understand the characterisation of hydration process, the kinetic models namely pseudo first order, pseudo second order and Avrami's fraction order model were adopted for all composites. Generally, the pseudo first order equation is better suited to describe the physical sorption processes. The equation is shown in Eq. (3).

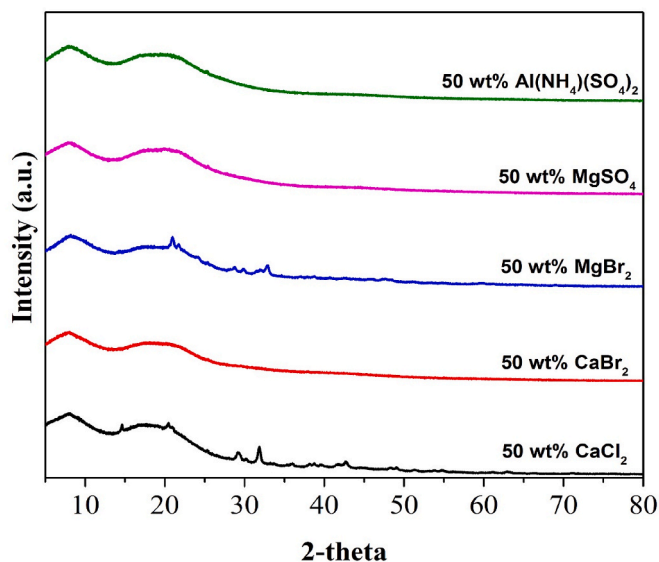


Fig. 7. XRD pattern for salt composites with salt loading level of 50 wt%.

$$q_t = q_e \cdot (1 - e^{-(K_1 \cdot x)}) \quad (3)$$

where q_t and q_e is the adsorption amount at time t and equilibrium state, K_1 is the rate constant for pseudo first order equation. x is the variable represents time elapsed.

The pseudo second order equation is generally used to describe the chemical sorption process such as moisture adsorption by salt samples.

The detailed equation is in Eq. (4).

$$q_t = \frac{q_e^2 \cdot K_2 \cdot x}{1 + q_e \cdot K_2 \cdot x} \quad (4)$$

where K_2 is the rate constant for pseudo second order equation.

The Avrami's equation can be adopted for those combinations of physical and chemical sorption processes. Its equation is shown in Eq. (5).

$$q_t = q_e \cdot \left(1 - e^{-\frac{(K_a \cdot x)^n}{n}}\right) \quad (5)$$

where K_a is the rate constant for Avrami's fraction order equation. n is the Avrami's exponent.

3. Results and discussion

3.1. Characterization of different salt composites

The nitrogen adsorption isotherm and pore size distribution of mesoporous PQ silica are shown in Fig. 2. Clearly, PQ silica was found to have type IV isotherm with the type H1 hysteresis loop in the high relative pressure region, which is the characteristic of mesoporous materials with high pore size uniformity. PQ silica exhibits a meso-macroporous hierarchical structure with the pore size distribution between 10 and 100 nm. Most of the pores in PQ silica are large mesopores with the pore size centred between 20 and 40 nm. The presence of a small fraction of macropores (50–100 nm) could potentially facilitate the water diffusion in the pores especially at high salt loading levels. As shown in Table 1, the original PQ silica had a high surface area of 283 m²/g and a pore volume of 1.79 cm³/g with an average pore size of 27.4

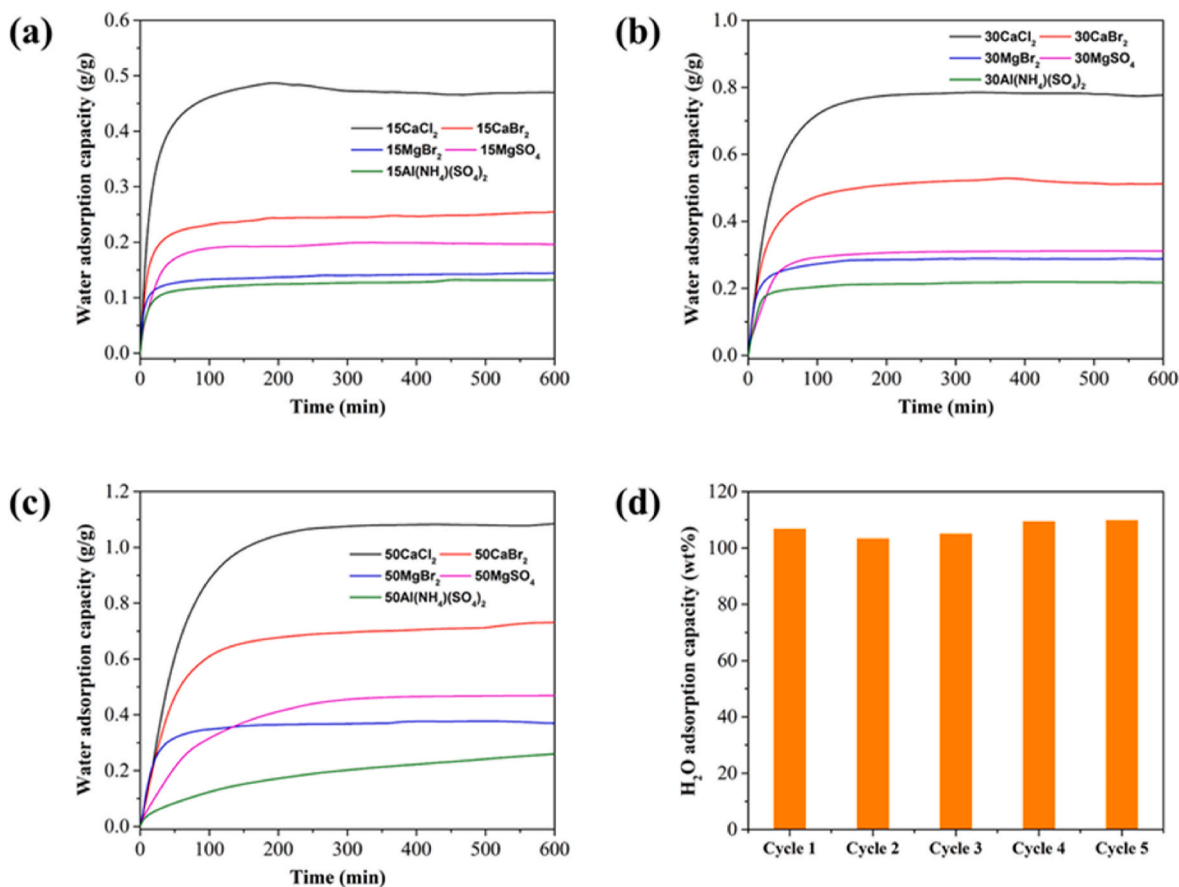


Fig. 8. Dynamic water adsorption capacity at 30 °C, 25 mBar for composites: (a) 15 wt% salt loading; (b) 30 wt% salt loading; (c) 50 wt% salt loading; (d) cycle stability test for 50CaCl₂.

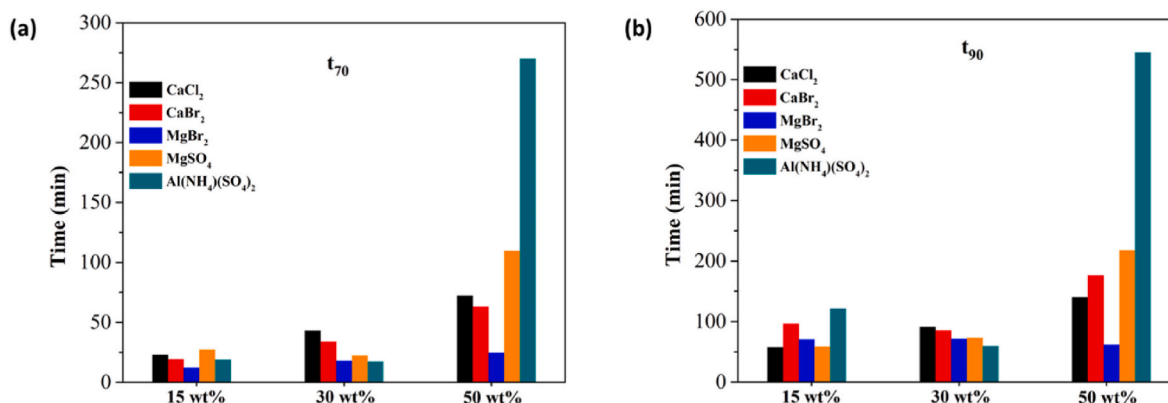


Fig. 9. Hydration kinetics of salt composites: time to achieve (a) 70% and (b) 90% of the equilibrium adsorption capacity.

Table 2

Adsorption kinetic results for salt composites.

Sample	Pseudo-first order			Pseudo-second order			Avrami's fraction-order			
	q_e	K_1	R^2	q_e	$K_2 \times 10^3$	R^2	q_e	K_a	n	R^2
15CaCl ₂	47.37%	0.049	0.97	48.63%	2.16	0.94	47.41%	0.041	0.83	0.99
15CaBr ₂	25.26%	0.054	0.81	25.97%	3.68	0.95	24.56%	0.031	0.62	0.98
15MgBr ₂	14.27%	0.084	0.71	14.61%	9.79	0.90	14.04%	0.025	0.48	0.96
15MgSO ₄	19.91%	0.040	0.94	20.51%	3.82	0.95	19.65%	0.037	0.86	0.99
15Al(NH ₄)(SO ₄) ₂	12.82%	0.062	0.82	13.26%	8.25	0.97	12.82%	0.021	0.52	0.97
30CaCl ₂	78.32%	0.027	0.99	81.97%	0.62	0.96	78.17%	0.026	0.95	1.00
30CaBr ₂	51.39%	0.033	0.98	53.38%	1.22	0.96	51.95%	0.024	0.77	0.99
30MgBr ₂	28.89%	0.059	0.90	29.67%	3.90	0.98	28.77%	0.033	0.64	0.99
30MgSO ₄	31.16%	0.033	0.99	32.45%	1.90	0.96	30.88%	0.033	0.99	0.99
30Al(NH ₄)(SO ₄) ₂	21.61%	0.060	0.95	22.23%	5.15	0.98	21.50%	0.044	0.76	0.97
50CaCl ₂	108.80%	0.016	0.99	117.30%	0.22	0.95	107.80%	0.018	1.10	1.00
50CaBr ₂	72.35%	0.018	0.97	77.21%	0.40	0.98	69.98%	0.020	0.98	1.00
50MgBr ₂	37.38%	0.041	0.93	38.62%	2.00	0.96	36.95%	0.034	0.81	0.98
50MgSO ₄	46.88%	0.011	1.00	51.38%	0.34	0.97	47.48%	0.010	0.92	1.00
50Al(NH ₄)(SO ₄) ₂	28.97%	0.004	0.96	35.90%	0.13	0.98	40.70%	0.001	0.59	1.00

nm. Previous studies have demonstrated that mesoporous matrices with large pore volume and pore size can accommodate a large amount of salt and enhance the accessibility of salt in pores, which leads to both high water adsorption capacity and fast adsorption kinetics [27]. The large pore volume and pore size feature make PQ silica a potential candidate support to prepare high-performance salt composites.

To investigate the impact of different salt types and salt loading levels on the water performance of PQ silica based salt composite, 5 different salts including CaBr₂, MgBr₂, MgSO₄, CaCl₂, and Al(NH₄)(SO₄)₂ were used to prepare PQ silica based salt composites with various salt loading levels of 15, 30 and 50 wt%. Fig. 3 shows the nitrogen adsorption isotherms of all salt composites. It can be seen that the nitrogen isotherm of all samples remains the type H1 hysteresis loop at high relative pressure region, indicating the presence of mesoporosity in salt composites. However, the nitrogen adsorption capacity varied with the type of salt used and the salt loading level. For the same salt type, the increase of salt loading level led to a continuous decrease in nitrogen adsorption capacity due to the occupation of mesopores by salt molecules. Interestingly, at the same salt loading levels, the nitrogen adsorption capacity of salt composite varied with the type of salt used. MgBr₂ and Al(NH₄)(SO₄)₂ based salt composites exhibited much higher nitrogen adsorption capacity than the other salts at the same salt loading levels, suggesting the less pore space occupied by MgBr₂, and Al(NH₄)(SO₄)₂ molecules. In comparison, CaCl₂ based salt composites showed the lowest nitrogen adsorption capacity. The variation in nitrogen adsorption capacity of different salt composites might be attributable to the different densities and molecular structure of different salts. Fig. 4 shows the pore size distributions (PSDs) of different salt composites. It is

evident that the impregnation of salt into mesopores led to a sharp decrease in the peak intensity of mesopores especially for the large mesopores and small macropores. With the increase of salt loading level, the PSDs of salt composites became narrower and shifted towards smaller pore size regions with the major pore sizes being around 20 nm. This indicates that salt molecules are preferable to be loaded in large pores.

Table 1 summarises the textural properties of different salt composites. The occupation of pore space by salt molecules led to a decrease in both surface area and pore volume. For instance, the surface area and pore volume decreased from 283 m²/g and 1.79 cm³/g without salt loading to 179–234 m²/g and 0.86–1.33 cm³/g, respectively, at the salt loading level of 15 wt%. When the salt loading level reached 50 wt%, the surface area and pore volume were reduced to about 78–122 m²/g and 0.40–0.63 cm³/g, respectively. With the same salt loading levels, MgBr₂ and Al(NH₄)(SO₄)₂ based salt composites exhibited higher pore volume and surface area than the other salt composites. The higher composite pore volume could be attributed to the higher density and better dispersion of the impregnated salt, which resulted in the less occupied volume in the PQ silica. The reduction of mesopore-size was also observed by the salt impregnation while it remains at around 20 nm as the salt loading level increases from 15 to 50 wt%, which is consistent with the PSDs shown in Fig. 4. The above results suggest that large pore volume and pore size were preserved in salt composite with salt loading levels as high as 50 wt%, which will benefit both the water diffusion during hydration and dehydration process and the accessibility of salt inside pores and therefore enhance the water adsorption capacity and kinetics.

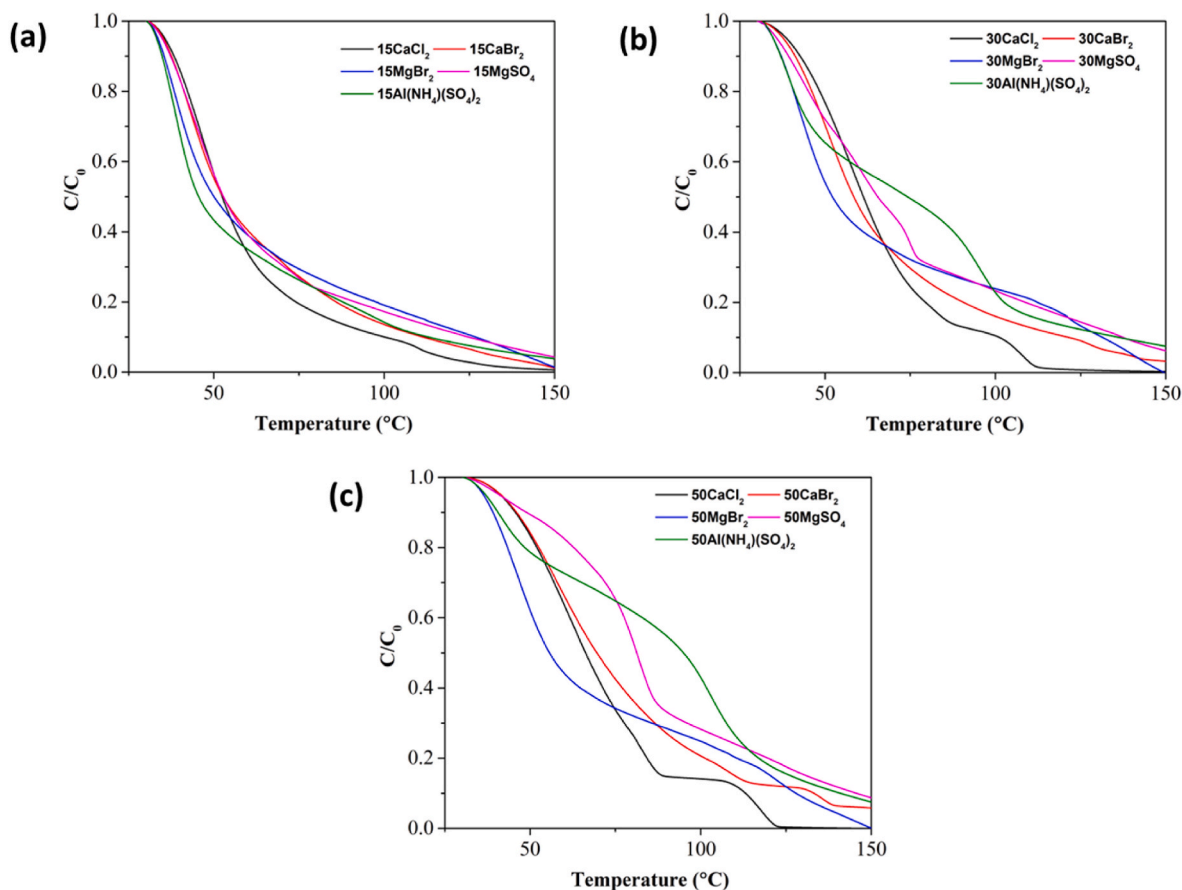


Fig. 10. Water desorption progress for composites under heating rate of 1 °C/min: (a) salt loading level of 15 wt% ; (b) salt loading level of 30 wt% ; (c) salt loading level of 50 wt% .

Table 3
Dehydration of different salts.

Salt sample	Reaction formula	Required temperature (°C)	Reference
CaCl ₂	CaCl ₂ ·6H ₂ O → CaCl ₂ ·4H ₂ O+2H ₂ O	room temperature	[41]
	CaCl ₂ ·4H ₂ O → CaCl ₂ ·2H ₂ O+2H ₂ O	63–142	
	CaCl ₂ ·2H ₂ O → CaCl ₂ +2H ₂ O	>142	
	CaBr ₂ ·6H ₂ O → CaBr ₂ ·4.5H ₂ O+1.5H ₂ O	room temperature	
CaBr ₂	CaBr ₂ ·6H ₂ O → CaBr ₂ ·4.5H ₂ O+1.5H ₂ O	room temperature	[42]
	CaBr ₂ ·4.5H ₂ O → CaBr ₂ ·3.5H ₂ O + H ₂ O	50–90	
	CaBr ₂ ·3.5H ₂ O → CaBr ₂ ·2H ₂ O+1.5H ₂ O	90–125	
	CaBr ₂ ·2H ₂ O → CaBr ₂ ·H ₂ O + H ₂ O	125–150	
MgBr ₂	CaBr ₂ ·H ₂ O → CaBr ₂ +H ₂ O	>150	[43]
	MgBr ₂ ·6H ₂ O → MgBr ₂ ·4H ₂ O+2H ₂ O	27–76	
	MgBr ₂ ·4H ₂ O → MgBr ₂ ·2H ₂ O+2H ₂ O	59–94	
	MgBr ₂ ·2H ₂ O → MgBr ₂ ·H ₂ O + H ₂ O	88–107	
MgSO ₄	MgBr ₂ ·H ₂ O → MgBr ₂ +H ₂ O	102–117	[44]
	MgSO ₄ ·7H ₂ O → MgSO ₄ ·6H ₂ O + H ₂ O	room temperature	
	MgSO ₄ ·6H ₂ O → MgSO ₄ ·0.2H ₂ O+5.8H ₂ O	47–275	
	MgSO ₄ ·0.2H ₂ O → MgSO ₄ +0.2H ₂ O	>275	
	MgSO ₄ +0.2H ₂ O		

Fig. 5 presents the morphology of selected PQ silica-based salt composites at different microscopic scales. The commercial PQ silica was in the form of irregular particles and the morphology was well preserved after salt impregnation. At the salt loading level of 15 wt%, the porous structure of PQ silica can still be observed. However, almost all pores were occupied by salt molecules at the high loading level of 50 wt% and similar phenomena were observed for the different salts as shown in Fig. 5 (d-l). To further investigate the porous textural features, Fig. 6 shows the high-resolution TEM images of PQ silica and its selected salt composites. It can be seen that the PQ silica exhibited a relatively ordered mesoporous structure. In comparison, salt impregnation makes the borders of mesopores become blurry especially at the high salt loading level of 50 wt%, which was lost due to the salt impregnation, indicating that the space of the pores was occupied by salt molecules, which is in agreement with the observation by Silvester et al. [39]. The distribution of silica and salt (e.g. CaCl₂) was investigated by using STEM-EDX surface elemental mapping is shown in Fig. 6 (g-h). Where green and purple represent the existence of silicon and calcium, respectively, with brightness indicating concentration. It can be seen that the concentration of silicon is much higher than calcium. The lower concentration of calcium in most areas indicates that CaCl₂ is inside the PQ silica. Interestingly, in some of the areas as highlighted in the figure, the concentration profile of silicon is opposite to calcium, the high concentration of calcium is due to the entrance of open pores at that area. The above phenomena suggest that the salt molecules were successfully loaded into the porous structure. This can be further verified by the surface elemental concentration shown in Fig. 6 (i) that the concentration of silicon and oxygen is much higher than calcium and chloride.

Fig. 7 shows the XRD pattern of salt composites with the salt loading

Table 4
Comparison of different salt composites by previous studies.

Sample name	Loading (wt %) ^a	Hydration temperature (°C)	Water vapour pressure (mBar)	Adsorption capacity (g/g)	t ₇₀ ^b	t ₉₀ ^b	Matrix pore size (nm)	Particle size (µm)	Reference
PQ silica + MgSO ₄	50	30	25.0	0.47	110	219	27.4	150–300	This paper
PQ silica + MgBr ₂	50	30	25.0	0.37	24.5	62	27.4	150–300	This paper
PQ silica + CaCl ₂	50	30	25.0	1.08	71	135	27.4	150–300	This paper
MCF + MgSO ₄	50	30	25.0	0.50	48	160	19.8–29.0	–	[27]
Silica + CaCl ₂	35	30	33.9	0.73	130	346	6.1	–	[23]
Silica + CaCl ₂	15	20	7.0	0.27	350	567	6.0	–	[45]
SBA15+CaCl ₂	60	25	9.5	0.70	460	675	7.0–8.0	0.67	[39]
MIL-101(Cr)+Na ₂ S ₂ O ₃	30	30	12.7	0.053	55	150	2.16	–	[46]
Zeolite + MgSO ₄	9	25	25.0	0.26	420	678	0.3–1	2000–3000	[13]
Silica + CaCl ₂	33.7	28	23.4	0.75	–	–	7.5	–	[47]
Silica + CaCl ₂	17	25	12.3	0.33	–	–	8.2	–	[48]
Silica + CaCl ₂	33	27	35.3	0.85	–	–	8.2	–	[48]
Silica + CaCl ₂	43	30	12.5	0.40	–	–	13.0	74	[24]
Silica aerogel + CaCl ₂	30	25	25.3	1.20	–	–	5.0–40.0	2000–5000	[37]
Silica xerogel + CaCl ₂	30	25	25.3	1.15	–	–	5.0–40.0	2000–5000	[37]
MIL-101(Cr)+CaCl ₂	63	30	12.5	0.30	–	–	–	–	[21]
expanded graphite + MgSO ₄	60	25	27.0	0.37	–	–	–	–	[49]
Zeolite + MgSO ₄	15	30	21.0	0.15	–	–	0.8–0.9	2000	[17]
Zeolite + MgSO ₄	8	25	25.0	0.27	–	–	3.4	3000–5000	[35]
Silica + Ca(NO ₃) ₂	45	30	12.4	0.55	–	–	15.0	–	[50]

^a The optimum salt loading level after the data analysis by the other authors.

^b The obtained value is estimated based on the hydration curve from literatures.

level of 50 wt%. The two low-intensity diffuse peaks detected in all the samples are attributed to the non-crystalline mesoporous PQ silica, which indicates the salt impregnation did not change the structure of PQ silica. It can be seen that there are only limited peaks observed for all composites at high salt loading level of 50 wt%, suggesting that the impregnated salt is either amorphous or liquid [39]. Some small peaks observed for 50MgBr₂ at 20.9° and 32.9° is attributable to MgBr₂ while the peaks centred at 14.7°, 29.4°, 31.9°, and 42.9° for 50CaCl₂ can be assigned to CaCl₂.

3.2. Moisture adsorption performance

The water adsorption performance of different salt composites was evaluated by using TGA at 30 °C and 25 mbar vapour pressure. The water adsorption profiles of different salt composites are shown in Fig. 8 (a-c). All the salt composites showed increased water adsorption capacity with the increase of salt loading level, while there was significant variation in water adsorption among different salt composites. The different moisture adsorption capacity/rate is determined by the water adsorption characteristics of different salts. At the same salt loading levels, the calcium-based salt composites exhibited higher water adsorption capacity than others. Specifically, CaCl₂ based salt composite showed the highest water adsorption capacity, from about 48 wt% at the salt loading level of 15 wt% to about 109 wt% at the salt loading level of 50 wt%. Assuming that all the CaCl₂ and CaBr₂ molecules were completely hydrated to hexahydrate, the maximum water adsorption capacity of salt composite containing 50 wt% CaCl₂ or CaBr₂ was about 48% and 27%, respectively, which was much lower than the water adsorption capacity obtained in this study. This could be attributed to the easy deliquescence of CaCl₂ and CaBr₂ at relatively high moisture pressures [40]. At 30 °C and vapour pressure of 25 mbar, the salts deliquesced into aqueous CaCl₂ and CaBr₂ inside the pores. The deliquescence of magnesium based salt and Al(NH₄)(SO₄)₂ was not detected in this study. Amongst all the salt composites, Al(NH₄)(SO₄)₂ based salt composites exhibited the lowest water adsorption capacity, which was only around 20 wt%. The cyclic stability of salt composite is critical in determining their life-time performance in practical applications.

Therefore, the best-performing PQ silica salt composites containing 50 wt% CaCl₂ was selected for cyclic testing at 30 °C and vapour pressure of 25 mbar. It can be seen from Fig. 8 (d) that the water adsorption capacity changed insignificantly over the 5 cycles of adsorption-desorption tests, highlighting the good adsorption reversibility and durability for water adsorption of PQ based salt composites.

It can be seen from Fig. 8 (a-c) that the water adsorption process of the PQ based salt composites can be divided into two stages: a linear water adsorption process followed by a slow adsorption process where the salt composites only achieved marginal increases in water adsorption capacity over a long time. It is obvious that the adsorption rate slowed down with the increasing salt loading level. To further evaluate the adsorption kinetics, the times taken to achieve 70% (t₇₀) and 90% (t₉₀) of the equilibrium adsorption capacity for different salt composites were calculated, as shown in Fig. 9. It can be seen that t₇₀ and t₉₀ varied with not only the salt loading level but also the type of salt. At the salt loading level of 15 wt%, the MgBr₂ based salt composite had the shortest t₇₀, being only 12.2 min while the CaCl₂ based salt composite spent less time to reaching 90% of the equilibrium water adsorption capacity than the other salt composites. According to Fig. 9, with the further increase of salt loading level, the MgBr₂ based salt composite was found to exhibit faster water adsorption rates, as indicated by its t₇₀ and t₉₀, which were shorter than those of the other salt composites. For instance, at the salt loading level of 50 wt%, the t₇₀ and t₉₀ of the MgBr₂ based salt composite were 24.5 and 62.0 min, respectively, which were less than 40% of the other salt composites. This can be attributed to its high surface and pore volume persevered after salt loading as shown in Table 1. It is also notable that the t₇₀ and t₉₀ of the MgSO₄ and Al(NH₄)(SO₄)₂ based composites sharply increased as the salt loading level increased from 30 to 50 wt% especially for Al(NH₄)(SO₄)₂ with t₉₀ being over 545 min. This suggests that the impregnation of MgSO₄ and Al(NH₄)(SO₄)₂ at a higher salt loading level of 50 wt% tends to partially block the pores of PQ silica and increase the thickness of the salt layer on the pore surfaces, making the diffusion of water molecules become slower. To further evaluate the water adsorption kinetics of the salt composites, three kinetic models including pseudo-first-order model, pseudo-second-order model and Avrami's fraction-order model, were

used to fit their adsorption curves and the fitting results are shown in Table 2.

It is found that Avrami's fraction-order model showed the best fitting result as the correlation coefficients of Avrami's fraction-order model were higher than the other two models, suggesting that the water adsorption in the PQ based salt composites is a complex process involving both physical and chemical interactions. The rate constant, K_a , an indicator of adsorption kinetics, decreased with the increasing salt loading level, which is mainly attributed to the continuously reduced accessibility of salt molecules in pores and enhanced water diffusion resistance. In contrast, K_a of the $MgBr_2$ based salt composites slightly increased with the increasing salt loading level. This is due to the large surface area and pore volume leading to good accessibility of $MgBr_2$ in pores and high water diffusivity.

3.3. Desorption performance

Dehydration kinetics is a critical parameter for evaluating the charging process of the salt composites. Fig. 10 shows the dehydration profiles of different salt composites as a function of temperature from 30 °C to 150 °C at the heating rate of 1 °C/min. Generally, the dehydration properties of salt composites were determined by the salt loading level as well as the properties of the salts. The dehydration stages of different salts reported in previous studies are shown in Table 3.

Most of the water in salt hydrate could be desorbed at about 150 °C whereas the dehydration process varies at different temperatures. However, as shown in Fig. 10, at the loading level of 15 wt%, all the salt composites exhibited similar desorption profiles as the water was quickly desorbed with increasing temperature, and over 80% of the water was desorbed at temperatures below 90 °C. The two main factors, which determine the dehydration process, are the breaking of chemical bonds between water/salt and the diffusion of water from salt to outside. At low salt loading levels, the well dispersion of salt molecules on pore walls minimized the diffusion resistance of desorbed water while the bond energy between salt and water was similar among different salts, so similar dehydration behaviours of different salt composites were observed. However, with increasing salt loading level, the diffusion resistance within the salt layer increased owing to the increasing thickness of the salt layer. Therefore, the dehydration temperature shifted towards a higher temperature region. Interestingly, all the $MgBr_2$ based salt composites had similar dehydration profiles, which is attributable to the good accessibility of salt molecules and the reduced water diffusion resistance in pores at all loading levels. The sharp increase of water diffusion resistance due to the partial blockage of pores by $MgSO_4$ and $Al(NH_4)(SO_4)_2$ at high salt loading levels led to a sharp increase in dehydration temperature. It can be seen from Fig. 10 that most of the PQ based salt composites can be potentially used for low temperature region as about 70–80% of the water could be desorbed at temperatures below 90 °C. This suggests that those materials could be potentially applied to store low grade heat or renewable energy such as industrial waste heat and solar energy.

4. Comparison of salt composites prepared using different porous matrices

The above results demonstrated that salt composites prepared by using PQ showed excellent water hydration/dehydration performance. Table 4 summarises the hydration/dehydration performance of salt composites with optimum or maximum salt loading levels prepared in previous studies. Clearly, the water adsorption capacity of salt composites at the salt loading level of 50 wt% outperforms most of the salt composites reported in previous studies, which is even higher than those containing 60 wt% salt prepared by using SBA-15 with the pore size of only 7–8 nm. Moreover, the large pore size of PQ could facilitate water adsorption kinetics and reduce the water diffusion resistance in pore

channels especially at high salt loading levels. For instance, at the similar salt loading level of 50 wt%, the t_{70} and t_{90} of $CaCl_2$ composites prepared by using mesoporous silica with pore size below 10 nm was much higher than PQ silica-based composites in even higher moisture content. MCF with a larger pore size and pore volume than PQ silica exhibited a much higher adsorption rate at the $MgSO_4$ loading level of 50 wt%. In addition to pore size, the type of salt is also critical. As shown in Table 4, $MgBr_2$ based salt composites exhibited a much faster adsorption rate than other salts based composites. The above results suggest the importance of developing porous matrices with large pores size to prepare salt composites for thermochemical energy storage. The particle size of PQ silica ranges from 150 to 300 μm belonging to Geldart group B particles possesses good fluidisability. As shown in Table 4, there are no viable porous matrices in previous studies that meet the requirement of fluidisation. PQ silica-based salt composites offer the potential to design and develop the fluidised bed reactor-based system for low temperature TCES. Amongst the different salts used in this study, $CaBr_2$ and $MgBr_2$ that have been rarely used in previous studies to prepare salt composites exhibited excellent water hydration/dehydration performance in both capacity and kinetics, especially $MgBr_2$ with the fastest adsorption rate among all composites at the same loading level. Moreover, the activation dehydration temperature of $MgBr_2$ was much lower than other salts such as $MgSO_4$ and $CaCl_2$. $MgBr_2$ will be a potential candidate for low-grade heat (<100 °C) recovery or solar-driven TCES system.

5. Conclusions

In this study, a series of salt composites with different salt loading levels and different types of salt were prepared using mesoporous silica as the porous matrix via an incipient wet impregnation method. The results demonstrated that the mesoporous PQ silica with the large pore size and pore volume could accommodate a large amount of salt. The thermal gravity analysis showed that the calcium based composites presented strong hygroscopic properties than the magnesium based composites and the $Al(NH_4)(SO_4)_2$ composite. By taking the benefits of large pore in the mesoporous structure, PQ composites achieved a high adsorption amount during hydration process. Specifically, under the hydration conditions of 30 °C and 25 mbar, the 50 $CaCl_2$ composite achieved a water adsorption capacity of 109 wt%, and the 50 $MgSO_4$ composite had a water adsorption capacity of 47 wt%. In addition, the $MgBr_2$ and $CaCl_2$ composites had fastest moisture adsorption rate over the course of the moisture adsorption process. Specifically, the 15 $MgBr_2$ composite reached 70% of adsorption equilibrium in only 12.2 min. The dehydration experiments showed that most composites were capable to desorb 70–80% of moisture at temperature below 90 °C. The results of high moisture adsorption capacity and fast moisture adsorption rate indicated that the mesoporous PQ silica composites could potentially be used for low-temperature thermal storage applications. Future work will be carried out to investigate the thermal energy storage performance by purpose-designed fluidised bed reactor.

Credit author statement

Haomin Wang: Writing – review & editing, Writing – original draft, Methodology, Investigation, Data curation. Xin Liu: Writing – review & editing, Methodology, Investigation, Data curation, Supervision. Xiao Liu: Writing – review & editing, Methodology. Chenggong Sun: Writing – review & editing. Yupeng Wu: Writing – review & editing, Supervision, Resources, Methodology, Funding acquisition.

Declaration of competing interest

The authors declare that they have no known competing financial interests or personal relationships that could have appeared to influence the work reported in this paper.

Data availability

Data will be made available on request.

Acknowledgement

This work was supported by the Engineering and Physical Sciences Research Council, UK [grant number EP/S030786/1] and the Centre for Postdoctoral Development in Infrastructure Cities and Energy Sandpit. This work was also supported by the Engineering and Physical Sciences Research Council (EPSRC) [under grants EP/L022494/1 and EP/W006413/1] and the University of Nottingham. The authors thank Dr. Michael Fay for his help with TEM analysis and Dr. Hannah Constantin and Ms Rebecca Saint for carrying out the XRD analysis.

References

- IEA. World energy outlook 2021. IEA: Population (Paris); 2021, p. 146–149.
- Salgado-Pizarro R, Calderón A, Svobodova-Sedlackova A, Fernández AI, Barreneche C. The relevance of thermochemical energy storage in the last two decades: the analysis of research evolution. *J Energy Storage* 2022;51:104377. <https://doi.org/10.1016/j.est.2022.104377>.
- Zhao Y, Zhao CY, Markides CN, Wang H, Li W. Medium- and high-temperature latent and thermochemical heat storage using metals and metallic compounds as heat storage media: a technical review. *Appl Energy* 2020;280:115950. <https://doi.org/10.1016/j.apenergy.2020.115950>.
- Lefebvre D, Tezel FH. A review of energy storage technologies with a focus on adsorption thermal energy storage processes for heating applications. *Renew Sust Energ Rev* 2017;67:116–25. <https://doi.org/10.1016/j.rser.2016.08.019>.
- Donkers PAJ, Sögütoglu LC, Huinink HP, Fischer HR, Adan OCG. A review of salt hydrates for seasonal heat storage in domestic applications. *Appl Energy* 2017;199:45–68. <https://doi.org/10.1016/j.apenergy.2017.04.080>.
- Posern K, Kaps C. Humidity controlled calorimetric investigation of the hydration of MgSO₄ hydrates. *J Therm Anal Calorim* 2008;92(3):905–9. <https://doi.org/10.1007/s10973-007-8640-4>.
- Mahon D. Investigation into the potential of MgSO₄ for interseasonal domestic thermochemical energy storage. Loughborough University; 2018.
- Zondag HA, Van essen M, Bleijendaal L, Kikkert B, Bakker M. Application of MgCl₂·6H₂O for thermochemical seasonal solar heat storage. *Petten: ECN* 2010.
- Zhao YJ, Wang RZ, Zhang YN, Yu N. Development of SrBr₂ composite sorbents for a sorption thermal energy storage system to store low-temperature heat. *Energy* 2016;115:129–39. <https://doi.org/10.1016/j.energy.2016.09.013>.
- H Abedin A, A Rosen M. A critical review of thermochemical energy storage systems. *Open Renew Energy J* 2011;4(1). <https://benthamopen.com/contents/pdf/TOREJ/TOREJ-4-42.pdf>.
- van Essen WMJ, Cot Gores J, Bleijendaal LPJ, Zondag HA, Schuitema R, Bakker M, van Helden WGJ. Characterization of Salt Hydrates for Compact Seasonal Thermochemical Storage 2009;(48906):825–30. <https://doi.org/10.1115/ES2009-90289>.
- Bales C, Gantenbein P, Hauer A, Henning H-M, Jaenig D, Kerskes H, Núñez T, Visscher K. Thermal properties of materials for thermo-chemical storage of solar heat. *IEA SHC*; 2005. p. 32.
- Xu C, Yu Z, Xie Y, Ren Y, Ye F, Ju X. Study of the hydration behavior of zeolite-MgSO₄ composites for long-term heat storage. *Appl Therm Eng* 2018;129:250–9. <https://doi.org/10.1016/j.applthermaleng.2017.10.031>.
- Zondag H, Kikkert B, Smeding S, Bakker M. Thermochemical seasonal solar heat storage with MgCl₂·6H₂O: first upscaling of the reactor. In: IC-SES conference; 2011.
- Gordeeva LG, Aristov YI. Composites ‘salt inside porous matrix’ for adsorption heat transformation: a current state-of-the-art and new trends. *Int J Low Carbon Technol* 2012;7(4):288–302. <https://doi.org/10.1093/ijlct/cts050>.
- Gordeeva L, Grekova A, Krieger T, Aristov Y. Composites “binary salts in porous matrix” for adsorption heat transformation. *Appl Therm Eng* 2013;50(2):1633–8. <https://doi.org/10.1016/j.applthermaleng.2011.07.040>.
- Hongois S, Kuznik F, Stevens P, Roux J-J. Development and characterisation of a new MgSO₄-zeolite composite for long-term thermal energy storage. *Sol Energy Mater Sol Cells* 2011;95(7):1831–7. <https://doi.org/10.1016/j.solmat.2011.01.050>.
- Whiting G, Grondin D, Bennici S, Aroux A. Heats of water sorption studies on zeolite-MgSO₄ composites as potential thermochemical heat storage materials. *Sol Energy Mater Sol Cells* 2013;112:112–9. <https://doi.org/10.1016/j.solmat.2013.01.020>.
- Tso CY, Chao CYH. Activated carbon, silica-gel and calcium chloride composite adsorbents for energy efficient solar adsorption cooling and dehumidification systems. *Int J Refrig* 2012;35(6):1626–38. <https://doi.org/10.1016/j.ijrefrig.2012.05.007>.
- Casey SP, Elvins J, Riffat S, Robinson A. Salt impregnated desiccant matrices for ‘open’ thermochemical energy storage—selection, synthesis and characterisation of candidate materials. *Energy Build* 2014;84:412–25. <https://doi.org/10.1016/j.enbuild.2014.08.028>.
- D’Ans P, Courbon E, Permyakova A, Nouar F, Simonnet-Jégat C, Bourdreux F, et al. A new strontium bromide MOF composite with improved performance for solar energy storage application. *J Energy Storage* 2019;25:100881. <https://doi.org/10.1016/j.est.2019.100881>.
- Gordeeva LG, Grekova AD, Krieger TA, Aristov YI. Adsorption properties of composite materials (LiCl+LiBr)/silica. *Microporous Mesoporous Mater* 2009;126(3):262–7. <https://doi.org/10.1016/j.micromeso.2009.06.015>.
- Zhu D, Wu H, Wang S. Experimental study on composite silica gel supported CaCl₂ sorbent for low grade heat storage. *Int J Therm Sci* 2006;45(8):804–13. <https://doi.org/10.1016/j.ijthermalsci.2005.10.009>.
- Courbon E, D’Ans P, Permyakova A, Skrylnyk O, Steunou N, Degrez M, et al. Further improvement of the synthesis of silica gel and CaCl₂ composites: enhancement of energy storage density and stability over cycles for solar heat storage coupled with space heating applications. *Sol Energy* 2017;157:532–41. <https://doi.org/10.1016/j.solener.2017.08.034>.
- Courbon E, D’Ans P, Permyakova A, Skrylnyk O, Steunou N, Degrez M, et al. A new composite sorbent based on SrBr₂ and silica gel for solar energy storage application with high energy storage density and stability. *Appl Energy* 2017;190:1184–94. <https://doi.org/10.1016/j.apenergy.2017.01.041>.
- Katiyar A, Yadav S, Smirniotis PG, Pinto NG. Synthesis of ordered large pore SBA-15 spherical particles for adsorption of biomolecules. *J Chromatogr A* 2006;1122(1):13–20. <https://doi.org/10.1016/j.chroma.2006.04.055>.
- Liu X, Wang H, Liu X, Yang F, Guan L, Sani S, et al. Development of MgSO₄/mesoporous silica composites for thermochemical energy storage: the role of porous structure on water adsorption. *Energy Rep* 2022;8:4913–21. <https://doi.org/10.1016/j.egy.2022.03.137>.
- Posern K, Linnow K, Niermann M, Kaps C, Steiger M. Thermochemical investigation of the water uptake behavior of MgSO₄ hydrates in host materials with different pore size. *Thermochim Acta* 2015;611:1–9. <https://doi.org/10.1016/j.tca.2015.04.031>.
- Dawoud B, Aristov Y. Experimental study on the kinetics of water vapor sorption on selective water sorbents, silica gel and alumina under typical operating conditions of sorption heat pumps. *Int J Heat Mass Transf.* 2003;46(2):273–81. [https://doi.org/10.1016/S0017-9310\(02\)00288-0](https://doi.org/10.1016/S0017-9310(02)00288-0).
- Zheng X, Ge TS, Wang RZ, Hu LM. Performance study of composite silica gels with different pore sizes and different impregnating hygroscopic salts. *Chem Eng Sci* 2014;120:1–9. <https://doi.org/10.1016/j.ces.2014.08.047>.
- Bu X, Wang L, Huang Y. Effect of pore size on the performance of composite adsorbent. *Adsorption* 2013;19(5):929–35. <https://doi.org/10.1007/s10450-013-9513-8>.
- Roßkopf C, Haas M, Faik A, Linder M, Wörner A. Improving powder bed properties for thermochemical storage by adding nanoparticles. *Energy Convers Manag* 2014;86:93–8. <https://doi.org/10.1016/j.enconman.2014.05.017>.
- Angerer M, Becker M, Härzschel S, Kröper K, Gleis S, Vandersickel A, et al. Design of a MW-scale thermo-chemical energy storage reactor. *Energy Rep* 2018;4:507–19. <https://doi.org/10.1016/j.egy.2018.07.005>.
- Cocco R, Karri SR, Knowlton T. Introduction to fluidization. *Chem Eng Prog* 2014;110(11):21–9.
- Wang Q, Xie Y, Ding B, Yu G, Ye F, Xu C. Structure and hydration state characterizations of MgSO₄-zeolite 13x composite materials for long-term thermochemical heat storage. *Sol Energy Mater Sol Cells* 2019;200:110047. <https://doi.org/10.1016/j.solmat.2019.110047>.
- Tohidi SH, Ziaie F, Abdolmaleki A. Preparation and characterization of SiO₂-CaCl₂ nanocomposite by the sol-gel method. *Int J Eng* 2009;22:299–305.
- Gordeeva LG, Mrowiec-Bialon J, Jarzebski AB, Lachowski AI, Malinowski JJ, Aristov YI. Selective water sorbents for multiple applications, 8. sorption properties of CaCl₂-SiO₂ sol-gel composites. *React Kinet Catal Lett* 1999;66(1):113–20. <https://doi.org/10.1007/BF02475749>.
- Almendros-Ibáñez JA, Fernández-Torrijos M, Díaz-Heras M, Belmonte JF, Sobrino C. A review of solar thermal energy storage in beds of particles: packed and fluidized beds, vol. 192. *Sol Energy*; 2019. p. 193–237. <https://doi.org/10.1016/j.solener.2018.05.047>.
- Silvester L, Touloumet Q, Kamaruddin A, Chassagneux F, Postole G, Aroux A, et al. Influence of silica functionalization on water sorption and thermochemical heat storage of mesoporous SBA-15/CaCl₂ composites. *ACS Appl Energy Mater* 2021;4(6):5944–56.
- Gough RV, Chevrier VF, Tolbert MA. Formation of liquid water at low temperatures via the deliquescence of calcium chloride: implications for Antarctica and Mars. *Planet Space Sci* 2016;131:79–87. <https://doi.org/10.1016/j.pss.2016.07.006>.
- Rammelberg HU, Schmidt T, Ruck W. Hydration and dehydration of salt hydrates and hydroxides for thermal energy storage - kinetics and energy release. *Energy Proc* 2012;30:362–9. <https://doi.org/10.1016/j.egypro.2012.11.043>.
- Paulik J, Paulik F, Buzágh-Gere E, Arnold M. Thermogravimetric examination of the dehydration process of calcium bromide hydrate under quasi isothermal and quasi isobaric conditions. *Thermochim Acta* 1979;31(1):93–100.
- Dinnebier RE, Runčevski T, Sugimoto K. Dehydration of magnesium bromide hexahydrate studied by in situ X-ray powder diffraction. *Z anorg allg* 2013;639(1):59–64. <https://doi.org/10.1002/zaac.201200445>.
- Van Essen V, Zondag H, Schuitema R, Van Helden W, Rindt C. Materials for thermochemical storage: characterization of magnesium sulfate. In: *Proceedings Eurosun*; 2008.
- Jabbari-Hichri A, Bennici S, Aroux A. CaCl₂-containing composites as thermochemical heat storage materials. *Sol Energy Mater Sol Cells* 2017;172:177–85. <https://doi.org/10.1016/j.solmat.2017.07.037>.

- [46] Padamurthy A, Nandanavanam J, Rajagopalan P. Preparation and characterization of metal organic framework based composite materials for thermochemical energy storage applications. *Appl Surf Sci* 2022;11:100309. <https://doi.org/10.1016/j.apsadv.2022.100309>.
- [47] Aristov YI, Restuccia G, Cacciola G, Parmon V. A family of new working materials for solid sorption air conditioning systems. *Appl Therm Eng* 2002;22(2):191–204.
- [48] Cortés FB, Chejne F, Carrasco-Marín F, Pérez-Cadenas AF, Moreno-Castilla C. Water sorption on silica-and zeolite-supported hygroscopic salts for cooling system applications. *Energy Convers Manag* 2012;53(1):219–23.
- [49] Miao Q, Zhang Y, Jia X, Li Z, Tan L, Ding Y. MgSO₄-expanded graphite composites for mass and heat transfer enhancement of thermochemical energy storage. *Sol Energy* 2021;220:432–9. <https://doi.org/10.1016/j.solener.2021.03.008>.
- [50] Simonova IA, Freni A, Restuccia G, Aristov YI. Water sorption on composite “silica modified by calcium nitrate”. *Microporous Mesoporous Mater* 2009;122(1–3): 223–8.